Identification of Spring Parameters for Deformable Object Simulation

Bryn A. Lloyd, *Graduate Student Member, IEEE*, Gábor Székely, *Associate Member, IEEE* and Matthias Harders, *Member, IEEE*

Abstract—Mass spring models are frequently used to simulate deformable objects because of their conceptual simplicity and computational speed. Unfortunately, the model parameters are not related to elastic material constitutive laws in an obvious way. Several methods to set optimal parameters have been proposed, but so far only with limited success. We analyze the parameter identification problem and show the difficulties, which have prevented previous work from reaching wide usage. Our main contribution is a new method to derive analytical expressions for the spring parameters from an isotropic linear elastic reference model. The method is described and expressions for several mesh topologies are derived. These include triangle, rectangle and tetrahedron meshes. The formulae are validated by comparing the static deformation of the MSM with reference deformations simulated with the finite element method.

Index Terms—Mass spring system, deformable model, parameters, spring coefficients, identification, static.

◆

1 INTRODUCTION

THE simulation of deformable objects is central to computer graphics. Since the pioneering work by Terzopoulos et al. [1, 2] mass spring models (MSM) have been used to model deformable objects, *e.g.* for cloth simulation [3, 4], face animation [5] or soft tissue behavior in surgery training systems [6–8]. For these and similar applications, the MSM has certain advantages over alternative methods, such as the finite element method (FEM), which is often used to solve elasticity problems. Compared to linear FEM, which is approximately as fast, the MSM has the advantage that it is more robust to rotations and large deformations. Non-linear FEM which avoids these problems is on the other hand computationally prohibitive, especially when the mesh topology changes and condensation methods cannot be employed [9, 10]. For these reasons, the MSM remains one of the most popular approaches for real-time deformable object simulation.

Many applications of mass spring models have been described, but only little attention has been directed towards setting optimal model parameters (masses, spring stiffness and damping coefficients). In most papers the question of obtaining appropriate parameters is not mentioned. Typically they are set manually, by tuning until the visual appearance is pleasing.

In contrast to the MSM, the elasticity parameters in the constitutive equations have been obtained for many materials. For instance isotropic linear elastic material is defined by two parameters, the Young's modulus E and Poisson's ratio ν. The Young's modulus is the slope of the initial, linear elastic part of the stress-strain curve in compression or tension. The Poisson's ratio is the negative of the ratio of the lateral strain to uniaxial strain, in axial loading. It can be interpreted as a measure of compressibility. Values are in the range between -1 and 0.5. For tissue simulation the Poisson's ratio is close to 0.5 (nearly

incompressible), because of the high water content. Several authors have measured the Young's modulus of different types of soft tissue (*e.g.* [11, 12]).

While an acceptable approach to select the masses has been found [13], the problem of selecting the appropriate spring constants is still unsolved. It would be especially interesting, if we could directly use the measured elasticity parameters to set the parameters in the MSM. For this purpose it is necessary to find a method, which is able to establish a link between the mass spring model and the constitutive equations.

Two approaches to assign the parameter values have emerged in the literature. The first is a data-driven strategy, where measured deformations are used as reference data to estimate the parameters. The second method is to use the actual physical model as a reference and derive analytical expressions for the spring coefficients. Both have mainly focused on the static equilibrium, *i.e.* stiffness and eventually mass parameters have been estimated. In this contribution we present a method to identify the spring stiffness coefficients. In the rest of this section, we briefly review the related work for the data-driven and for the analytical approaches.

Data-Driven MSM Parameter Identification

The first strategy is data-driven using measured deformation data to estimate the optimal parameters. The graphics community has mostly tried to determine the parameters by comparing the appearance of the real object with the MSM using *e.g.* range data [14, 15]. A similar but physics-based approach uses reference deformations simulated with the FEM [13, 16, 17].

In the static equilibrium the MSM equations can be written as

$$\mathbf{f}^{ext} = \mathbf{f}(\mathbf{x}, \theta), \qquad (1)$$

where $\mathbf{f}(\mathbf{x}, \theta)$ is a $N \cdot d \times 1$ vector containing the spring forces, $\mathbf{x} = (\mathbf{p}_1, \mathbf{p}_2, \cdots, \mathbf{p}_i, \cdots, \mathbf{p}_N)$ is a $N \cdot d \times 1$ vector which contains all the d-dimensional vertex positions $\mathbf{p}_i$, and $\theta =$

• B. Lloyd is with the Computer Vision Laboratory, ETH Zürich, 8092 Zürich, Switzerland email: blloyd@vision.ee.ethz.ch

$(k_1, k_2, \cdots, k_j, \cdots, k_M)^T$ is a $M \times 1$ vector of the unknown spring stiffness coefficients. The vector $\mathbf{f}^{ext}$ on the left hand side contains the external forces at each node. Given the external forces $\mathbf{f}^{ref}$ and the corresponding vertex positions $\mathbf{p}^{ref}$ of a reference model in the deformed state, the goal is to optimize the spring coefficients so that the MSM and the reference model behave similarly. The quality criterion is usually defined as the Euclidean distance between the nodes of the learning and the reference model.

$$G(\theta) = \sum_i \left\| \mathbf{p}_i^{ref} - \mathbf{p}_i(\theta, \mathbf{f}^{ref}) \right\|^2,$$

where the positions $\mathbf{p}_i(\theta, \mathbf{f}^{ref})$ are the equilibrium positions for a specific parameter vector θ and given external forces $\mathbf{f}^{ref}$. $G(\theta)$ must be minimized to obtain optimal parameters $\hat{\theta}$. This involves computing the equilibrium positions for each candidate parameter vector θ. Classical optimization methods usually get trapped in local minima. Therefore, mostly alternative methods have been used. Deussen et al. [13] suggested a method based on Simulated Annealing. Bianchi et al. [16, 17] proposed to use Genetic Algorithms to optimize the objective function. Their contribution highlighted that MSM parameters can also include mesh topology, which they optimized together with the stiffness values. Both authors presented results for small meshes. It is likely that their methods would have difficulty with larger meshes with many unknown spring coefficients. Louchet et al. [14] used Evolutionary Algorithms to minimize $G(\theta)$. They reduced the complexity by using only 5 parameters for the complete model (specific to cloth animation). This allowed them to identify parameters for large meshes. Nogami et al. [18] used Genetic Algorithms to estimate parameters of stiffness and damping coefficients.

Various problems have prevented these methods from reaching wide usage, which will be discussed in Section 2.

Deriving Analytical Expressions

The second approach is to derive analytical expressions for the spring parameters. So far, only few contributions have been made in this research direction. Specifically, van Gelder [19] presented a formula for the spring coefficient, which can be used to approximate the behavior of linear elastic material. The formula is valid for triangle meshes, however, a similar expression for tetrahedral meshes is also suggested. Although it was derived in a heuristic way, it is able to give good results under certain conditions (see discussion in Section 3). A drawback of the method, is that it does not result in a better insight into the problem of selecting appropriate parameters and it is unclear which assumptions were made.

Maciel et al. [20] suggested a formula for non-linear springs in a hexahedral mesh. The stiffness parameter depends on the current angles between the springs and must be recomputed in every iteration. Etzmuss et al. [21] derived forces for a particle system, which is directly obtained from a either a membrane or a thin plate model, by discretizing the equations using a finite difference approach on a rectangular grid.

In a recent contribution Wang and Devarajan [22] presented some formulae for a MSM to simulate a 1D beam and 2D plate bending model. The model is supposed to provide correct bending and stretching resistance. In [23] they extend their approach by using angular springs to improve the lateral resistance. Their method is based on using explicit continuum expressions of the potential energy for a given object, e.g. for a flat circular plate. The object domain is discretized with a regular mesh (rectangular or equilateral triangle mesh) and the parameters of the mass spring model are optimized to approximate the energy term. Their conclusion is that a spring model with preload helps to improve the accuracy, because it increases the available degrees of freedom of the model. A spring with preload is an extension of the spring model, which introduces a modified rest-length of the spring. Due to the adjusted rest-length, the model is not in the static equilibrium in its original configuration.

In this contribution we present a new method to derive the stiffness parameters from a reference model. First the reference model is discretized by dividing the object into elements. The equations for the material behavior are then approximated using a finite element method. We then attempt to find an equivalent mass spring model for each element. The MSM equations are non-linear in the node positions, whereas the FEM for linear elasticity leads to equations that are linear in the node displacements. Therefore, we linearize the MSM equations, so that we can equate them with the FEM equations and solve for the spring coefficients. Like in the FEM, these MSM elements can be assembled to obtain the complete model. Our approach has several advantages. First, it results in explicit formulae for the MSM. Second, the conditions under which the formulae are valid, are explicitly stated as equations. If it is not possible to equate the element equations, we propose two solutions. Either the corresponding MSM element is extended to add an additional degree of freedom, or we define an error term, which can be minimized analytically in order to obtain expressions for the stiffness coefficients.

In the next section we explain some of the drawbacks of the data-driven approach. In Section 3 we use our method to derive spring coefficients for triangle mass spring meshes, simulating the plane stress problem. Expressions for different mesh topologies, including tetrahedral meshes, are derived in Section 4. Experimental results are presented in Section 5 and finally, in Section 6 we discuss the results and suggest future work.

2 ANALYSIS OF THE DATA-DRIVEN PARAMETER IDENTIFICATION METHODS

In this section we discuss the data-driven approach to estimate the MSM parameters. Related approaches described by Deussen et al. [13], Louchet et al. [14] and Bianchi et al. [17] mainly focus on the optimization method. The authors all use the same objective function, the Euclidean distance between corresponding points of the learning and the reference model. This is a natural choice, but it is responsible for several problems and is the main reason why classical optimization methods have not been used. Some of the difficulties are related to:

- Speed, stability, smoothness
- Local minima
- Negative spring coefficients
- Learning data acquisition

The evaluation of the objective function $G(\theta)$ can be slow, since we need to calculate the static equilibrium of the MSM for parameters θ and external forces $\mathbf{f}^{ref}$. Algorithms to calculate the equilibrium have been described in Brown et al. [8] or Deussen et al. [13]. These are iterative methods which usually depend on parameters such as the step size α and number of iterations n. On the one hand, if the step size α is too large the computation is not stable. On the other hand, it should be as large as possible, in order to reduce the computation time. A problem can occur when the parameters θ change and the system becomes stiffer, making the reduction of α necessary to avoid instability. If n is too small, the algorithm will not converge and the objective function will not be smooth, which can have an effect on the optimization method. Both the optimal n and the optimal α depend on the current parameters θ.

The problem of local minima and smoothness of the objective function is the reason why most attention has been directed towards Evolutionary and Genetic Algorithms. Negative spring stiffness parameters can be dealt with by limiting the search space to non-negative values. But then it is still possible that some springs have very small stiffness values, which can also be undesirable. Possible ways to solve this might be to define a reasonable search space. Alternatively, a penalty term could be added to the objective function, which for instance penalizes deviations from the mean spring stiffness value.

To overcome these difficulties we have experimented with various problem formulations, alternative objective functions and optimization methods. Rewriting Equation 1 as $\mathbf{f}^{ext} = \mathbf{f}(\mathbf{x}, \theta) = U(\mathbf{x}) \cdot \theta$ we obtain a simpler objective function

$$G_{new}(\theta) = \left\| \mathbf{f}^{ref} - U(\mathbf{x}^{ref}) \cdot \theta \right\|, \qquad (2)$$

where $U(\mathbf{x}^{ref})$ is a $N \cdot d \times M$ matrix, computed using the node positions in the reference deformations. $\mathbf{f}^{ref}$ are the applied forces, used to generate these deformations. The assumption made in Equation 2 is that the MSM can be in equilibrium at the same positions as the reference model for given external loads. Therefore, the residual forces should be close to zero for the given deformations and $G_{new}(\hat{\theta})$ should be as small as possible. This simplifies the optimization problem considerably, because the objective function is a simple linear least squares problem with only one minimum. The method performs well if the MSM is capable of closely approximating the reference model. Otherwise the Euclidean distance based objective function has a better performance.

The last item concerns the reference deformations, which are used as learning-data. It is for instance not always obvious how to apply equivalent external forces to the MSM. In addition, the estimated parameters $\hat{\theta}$ are sensitive to the choice of reference deformation examples. This is mainly due to the non-linearity of the MSM. In Figure 1 the force-displacement curves of a triangle (a) and rectangle (b) MSM are shown. The models are aligned with the x-axis and fixed at the bottom edge. In the case of the triangle model, an external force is applied at the top node. For the rectangle model equal forces are applied at both top nodes. As can be seen, the models are softer when compressed and stiffer when stretched. Computed values are displayed as circles. The solid lines represent a linear fitting
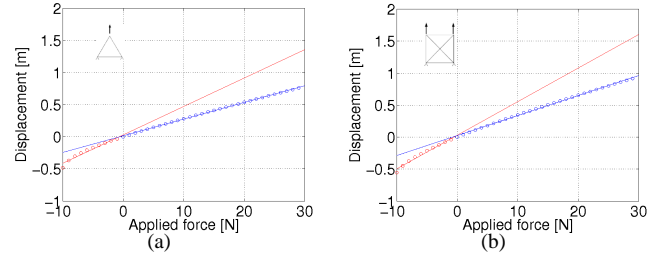

Fig. 1. The force-displacement non-linearity of mass spring models. Image (a) shows the relation for an equilateral triangle MSM with edge length 1m. Image (b) shows the corresponding relation for a square MSM with edge length 1m. The circles correspond to computed values.

function. The gradient of the linear fitting functions is a factor two larger for compression than for stretching. This behavior has not been observed for linear FEM. Therefore, a data-driven method should use measured data corresponding to small stretching, compression and shear deformations in all directions to reduce direction dependent bias. For arbitrary object shapes it is difficult to obtain reference deformations which provide unbiased data.

Finally, if topology changes must be made to the mesh, the whole identification procedure must be repeated. This is not compatible with interactive-time or real-time simulations.

3 SPRING STIFFNESS EXPRESSIONS FOR TRIANGULAR MESHES

The analytical approach is described in this section for the case of triangle meshes. In 1D the spring model is linear in the node positions. In higher dimensions this linearity is lost. By comparison, the linear elastic material equations in the FEM are linear in the node displacements $\mathbf{d}$. The MSM equations can be written as $\mathbf{f} = \mathbf{f}(\mathbf{x}) = \mathbf{f}(\mathbf{x}^0 + \mathbf{d})$, where $\mathbf{f}$ is a vector-valued function. The FEM equations are of the form $\mathbf{f} = K \mathbf{d}$, where K is the stiffness matrix. A maybe naive hope is that by linearizing the spring force as function of the positions (*i.e.* equivalently in the displacements), we can find the optimal spring parameters, such that both models are the same at least for small deformations. Equating the linearized mass spring model equations with the FEM equations is equivalent to equating the stiffness matrices. This results in a linear approximation in the operating point. Van Gelder [19] tried this approach but did not find a solution. We show here that there is an exact solution for equilateral triangles and one specific Poisson coefficient. For other cases an approximation can be found.

Four steps are necessary to derive the spring coefficients for a given topology. First, the element stiffness matrix must be calculated analytically using the FEM. Second, a MSM element with the same shape is selected. Then, the corresponding MSM equations are linearized and the stiffness matrix is derived. Finally, the stiffness matrices are equated. If this is not possible for the chosen MSM, a different or enhanced model should be chosen.

3.1 FEM Equations for a Triangle Element

In the FEM the continuous model is discretized by dividing the object into small interconnected regions, called finite elements. The constitutive laws are approximated by interpolation functions associated with each element. In the iso-parametric formulation these functions are called shape functions [24]. Force equilibrium equations are formulated per element and summed. A commonly used 2D element is the constant strain triangle (CST). It is also called the Turner-triangle or the 3-node triangle with linear displacement interpolation functions. The element equations can be written as

$$\mathbf{f}^e = K_{CST}\,\mathbf{d}^e,$$

where $\mathbf{f}^e$ is a vector containing the forces at the three nodes, K_{CST} is the stiffness matrix and $\mathbf{d}^e$ are the node displacements due to the forces $\mathbf{f}^e$. Throughout this paper we follow the convention that force and displacement vectors are ordered by node, *e.g.* the displacement vector is defined as $\mathbf{d}^e = (u_1, v_1, u_2, v_2, \cdots, u_N, v_N)$, where u_i and v_i are the displacements in x and y-direction respectively. The element stiffness matrix can be computed analytically. Logan [25] gives the explicit expression. It is presented here for convenience. Let t be the thickness of the plane stress elastic model, E the Young's modulus, ν the Poisson's ratio, (x_i, y_i) the coordinates of node i and A the area of the triangle. The plane stress assumptions are briefly explained in Appendix A. Assuming the triangle nodes in counterclockwise direction are $\mathbf{p}_i$, $\mathbf{p}_j$ and $\mathbf{p}_k$, the stiffness matrix is

$$K_{CST} = \begin{bmatrix} K_{i,i} & K_{i,j} & K_{i,k} \\ K_{j,i} & K_{j,j} & K_{j,k} \\ K_{k,i} & K_{k,j} & K_{k,k} \end{bmatrix} \tag{3}$$

where

$$K_{i,k} = \frac{tE}{4A(1+\nu)(1-\nu)} \tag{4}$$

$$\begin{bmatrix} \beta_i\beta_k + \gamma_i\gamma_k\left(\frac{1-\nu}{2}\right) & \beta_i\gamma_k\nu + \beta_k\gamma_i\left(\frac{1-\nu}{2}\right) \\ \beta_k\gamma_i\nu + \beta_i\gamma_k\left(\frac{1-\nu}{2}\right) & \gamma_i\gamma_k + \beta_i\beta_k\left(\frac{1-\nu}{2}\right) \end{bmatrix}. \tag{5}$$

The following variable substitution was used to simplify the expressions:

$$\begin{aligned} \beta_i &= y_j - y_k & \gamma_i &= x_k - x_j \\ \beta_j &= y_k - y_i & \gamma_j &= x_i - x_k \\ \beta_k &= y_i - y_j & \gamma_k &= x_j - x_i \end{aligned}$$

K_{CST} is a 6×6 symmetric matrix. The derivation is analogous to the derivation for the tetrahedron element shown in Appendix B.

3.2 Linearized Triangle MSM Force

We choose a triangle MSM consisting of the nodes $\mathbf{p}_i$, $\mathbf{p}_j$ and $\mathbf{p}_k$ connected by three springs as the corresponding model. The relationship is shown in Figure 2. In this section we linearize the model and derive its stiffness matrix. To make it easier to follow, we first linearize the force from a single spring (i,j) at node i in the static equilibrium. Using the intermediate result
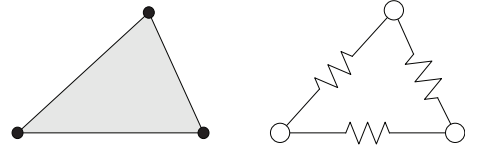

Fig. 2. On the left the FEM triangle element is shown. On the right the corresponding MSM is depicted.

we generalize to a triangle spring model. Using $\mathbf{p}_i = (x_i, y_i)^T$ the force at node i is

$$\begin{pmatrix} f_{(i,j),x} \\ f_{(i,j),y} \end{pmatrix} = k_{(i,j)}\left[(\mathbf{p}_i - \mathbf{p}_j)\left(1 - \frac{l^0_{(i,j)}}{\|\mathbf{p}_i - \mathbf{p}_j\|}\right)\right],$$

where $f_{(i,j),x}$ is the x-component of the force at node i from the spring (i,j). The variables $k_{(i,j)}$ and $l^0_{(i,j)}$ correspond to the spring coefficient and rest-length respectively. The first derivative of $f_{(i,j),x}$ with respect to x_i is

$$\frac{\partial f_{(i,j),x}}{\partial x_i} = k_{(i,j)}\left[\left(1 - \frac{l^0_{(i,j)}}{\|\mathbf{p}_i - \mathbf{p}_j\|}\right) + \frac{(x_i - x_j)^2\, l^0_{(i,j)}}{\|\mathbf{p}_i - \mathbf{p}_j\|^3}\right]$$

The first derivative of $f_{(i,j),x}$ with respect to y_i is

$$\frac{\partial f_{(i,j),x}}{\partial y_i} = k_{(i,j)}\frac{(x_i - x_j)(y_i - y_j)\, l^0_{(i,j)}}{\|\mathbf{p}_i - \mathbf{p}_j\|^3}$$

The derivatives of $f_{(i,j),y}$ with respect to x_i and y_i are

$$\frac{\partial f_{(i,j),y}}{\partial x_i} = k_{(i,j)}\frac{(y_i - y_j)(x_i - x_j)\, l^0_{(i,j)}}{\|\mathbf{p}_i - \mathbf{p}_j\|^3}$$

$$\frac{\partial f_{(i,j),y}}{\partial y_i} = k_{(i,j)}\left[\left(1 - \frac{l^0_{(i,j)}}{\|\mathbf{p}_i - \mathbf{p}_j\|}\right) + \frac{(y_i - y_j)^2\, l^0_{(i,j)}}{\|\mathbf{p}_i - \mathbf{p}_j\|^3}\right]$$

Since the force acting at node j is $\mathbf{f}_{(j,i)} = -\mathbf{f}_{(i,j)}$, it is straight forward to calculate the complete spring stiffness matrix. Assuming the spring is in static equilibrium, the stiffness matrix for a single spring can be written as

$$K_{S_{i,j}} = \begin{bmatrix} A_{i,j} & -A_{i,j} \\ -A_{i,j} & A_{i,j} \end{bmatrix} \tag{6}$$

where

$$\begin{aligned} A_{i,j} &= \frac{k_{(i,j)}}{l^0_{(i,j)}{}^2}\begin{bmatrix} \left(x^0_i - x^0_j\right)^2 & \left(x^0_i - x^0_j\right)\left(y^0_i - y^0_j\right) \\ \left(y^0_i - y^0_j\right)\left(x^0_i - x^0_j\right) & \left(y^0_i - y^0_j\right)^2 \end{bmatrix} \\ &= \frac{k_{(i,j)}}{l^0_{(i,j)}{}^2}\left(\mathbf{p}^0_i - \mathbf{p}^0_j\right)\left(\mathbf{p}^0_i - \mathbf{p}^0_j\right)^T. \end{aligned}$$

Alternatively, we could have derived the matrix $K_{S_{i,j}}$ using Equation 18 presented in Appendix C. It is the Hessian matrix of the potential energy of the spring with respect to the node positions.

We obtain the stiffness matrix of a triangle MSM by summing the stiffness matrices of each spring (since forces add)

$$K_{MSM} = \sum_{l,m} K_{S_{l,m}} = \begin{bmatrix} C_{i,i} & C_{i,j} & C_{i,k} \\ C_{j,i} & C_{j,j} & C_{j,k} \\ C_{k,i} & C_{k,j} & C_{k,k} \end{bmatrix} \tag{7}$$

where the summation is done in global coordinates. As an example the matrix $K_{S_{1,3}}$ in global coordinates is defined as

$$K_{S_{1,3}} = \begin{bmatrix} A_{1,3} & 0 & -A_{1,3} \\ 0 & 0 & 0 \\ -A_{1,3} & 0 & A_{1,3} \end{bmatrix}$$

Using Equations 6 and 7 we obtain

$$K_{MSM} = \begin{bmatrix} A_{i,j} + A_{i,k} & -A_{i,j} & -A_{i,k} \\ -A_{i,j} & A_{i,j} + A_{j,k} & -A_{j,k} \\ -A_{i,k} & -A_{j,k} & A_{i,k} + A_{j,k} \end{bmatrix}.$$

Since each sub-matrix $A_{i,j}$ is symmetric, the stiffness matrix of the triangle model is also symmetric.

3.3 Equating the Stiffness Matrices from FEM and the linearized MSM

Based on the expressions for the stiffness matrix of the constant strain triangle and the linearized MSM, we will attempt to calculate the parameters of the MSM. Since both matrices are symmetric, only the upper right triangular part of the matrices needs to be equated. This results in a 21×3 system of linear equations. In general the 2×2 sub-matrices $K_{i,j}$ are not symmetric (see Equation 3), whereas the corresponding matrices $C_{i,j}$ are always symmetric. However, if the Poisson's ratio ν is $\frac{1}{3}$ then $K_{i,j}$ becomes symmetric.

To simplify the equations we translated and rotated the triangle. After the transformation the node $\mathbf{p}_i$ is at the origin and $\mathbf{p}_j$ is on the x-axis. Additionally setting $\nu = \frac{1}{3}$ we obtain several equations, which express the condition that the triangle must be equilateral. Accepting this condition the system of equations can be solved for $k_{(i,j)}$. After transforming the coordinates back into the general coordinate system, we can show that

$$k_{(i,j)} = E\,t\frac{\sqrt{3}}{4},$$

Because the triangle is equilateral, the formulae for the other two springs are identical.

In order to obtain the stiffness matrix of the complete mesh, element stiffness matrices are added. Since a spring must model the stiffness contribution from both adjacent triangles (one if it is on the boundary), the final formula is

$$k_{(i,j)} = \sum_e E\,t\frac{\sqrt{3}}{4}, \tag{8}$$

where the sum is over the adjacent elements e.

3.4 Optimal Poisson's Ratio

Although the Poisson's ratio does not appear to have a large influence for small deformations, it is apparent that for a material with a Poisson's ratio close to $\frac{1}{3}$ the corresponding MSM with the derived spring parameters behaves more like the reference model than for instance $\nu = 0.0$. This is illustrated in Figure 3, where a membrane was simulated with a MSM and the FEM using different values of ν. The maximum node-distance error and the mean error is plotted against ν. In our derivation for the plane stress case a necessary condition to solve the system of equations was that $\nu = \frac{1}{3}$. Thus, the theoretical condition for ν is supported by experimental results.
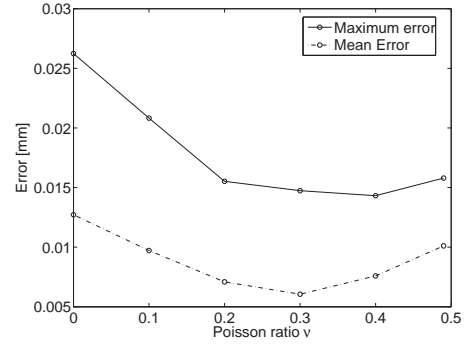

Fig. 3. Deformation of an object simulated with an equilateral triangle MSM compared to the simulation with FEM. The maximum deformation error and mean deformation error between the reference model and MSM is plotted for different values of ν. The object is a hexagon which is $1.7cm$ high (meshed with equilateral triangles).

3.5 Interpretation

Since van Gelder also derived a formula for triangle meshes, it is interesting to compare our result with his. His formula is $k_{(i,j)} = \sum_e E\,t\frac{A_e}{l^2_{(i,j)}}$, where A_e is the area of the triangle element e. For equilateral triangles this formula becomes equal to ours in Equation 8. However, in his paper van Gelder states this formula is valid for a Poisson's ratio of zero, whereas we have formally found the solution to be valid for $\nu = \frac{1}{3}$. Additionally, our experiments indicate that the MSM approximates a reference material with $\nu = \frac{1}{3}$ better than a material with $\nu = 0$ (see Figure 3). The fact that the MSM can only model one Poisson ratio should perhaps not come as a surprise. If we expect to control the Poisson ratio of a model using the stiffness coefficients, this should be possible without modifying the Young's modulus E. This is obviously not possible, since E and the stiffness coefficients are directly proportional.

Although van Gelder's claim that his formula is valid for a Poisson ratio of zero is false, there is some reasoning why it might be an improvement for general triangles. According to (8), the coefficient of a spring with two adjacent triangles is twice as large as the coefficient of a boundary spring with only one such triangle. This is because it must model the stiffness contribution of the material in both triangles. We conclude that the area of the adjacent triangles contributes to the stiffness of the springs. Similarly, van Gelder's formula can be rewritten and interpreted as

$$k_{(i,j)} = \sum_e Et\frac{\sqrt{3}}{4}\frac{A_e}{A_0}, \tag{9}$$

where A_0 is the size of an equilateral triangle with edge length $l_{(i,j)}$. We can see the terms of the sum have been scaled by $\frac{A_e}{A_0}$ compared to our formula in (8), *i.e.* the area of the adjacent triangles are taken into account. Although this is not an exact solution, we propose to use it as a approximation for arbitrary triangle shapes. Please note that example deformantions are shown in Section 5.

4 FORMULAE FOR OTHER MESH TOPOLOGIES

Van Gelder [19] was able to derive a formula for the spring coefficients for triangle meshes and heuristically for tetrahedral meshes. He did not attempt to find similar expressions for other mesh topologies or possibly other types of forces, *e.g.* volume preserving forces. Indeed, it is not obvious how his approach could be generalized.

Using the approach described in the previous section, we first derive formulae for 2D rectangular, and then for 3D tetrahedral spring meshes. In both cases it is not as straight forward to find expressions for the spring coefficients as for the triangular mesh. In the rectangle case, we extend the MSM in order to obtain a better match between stiffness matrices of the MSM and the FEM-based reference model. In the tetrahedron case we are however not able to find a perfect match. For this reason, we introduce a similarity criterion, which can be optimized analytically.

4.1 Rectangle Elements

As in the previous section we first calculate the element stiffness matrix using a finite element method, then derive the stiffness matrix of the corresponding linearized MSM and finally compute the spring stiffness expressions.

Logan [25] gives a brief description on how to calculate the 8×8 stiffness matrix K_{FEM} of the 4-node rectangle element with Lagrangian (bilinear) shape functions for the plane stress problem. The corresponding MSM is assumed to consist of six springs, *i.e.* four edge springs and two diagonal springs. The corresponding model is fully connected, meaning each node is connected to all other nodes of the rectangle element via springs. The relationship is shown in Figure 4. The stiffness
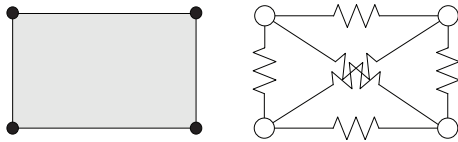

Fig. 4. On the left the FEM rectangle element is shown. On the right the corresponding MSM is depicted.

matrix of the linearized rectangle MSM can again be derived by summing the stiffness matrices of the individual springs (see Equation 7).

$$K_{MSM} = K_{S_{1,2}} + K_{S_{2,3}} + K_{S_{3,4}} + K_{S_{4,1}} + K_{S_{1,3}} + K_{S_{2,4}}$$

We calculated the matrices K_{FEM} and K_{MSM} using the MATLAB Symbolic Math Toolbox [26]. Due to space considerations they cannot be given here.

In order to analyze the stiffness matrices, we assume that the element is aligned to the x-axis and y-axis with side lengths a and b. Unfortunately, K_{MSM} is sparse, whereas in general the FEM stiffness matrix K_{FEM} contains no zeros. It would seem that the stiffness matrices K_{MSM} and K_{FEM} cannot be equated. By closer inspection, we found that the equations resulting from the zero elements in the main diagonal and the side-diagonals with index sum $i + j = 5$ and $i + j = 13$ can be satisfied, if the Poisson's ratio is $\frac{1}{3}$. Additionally, as in the triangle case this value makes the sub-matrices $K_{i,j}$ symmetric.

The remaining zero elements however, lead to conditions which are not plausible (*e.g.* Young's modulus $E = 0$). In order to find an exact solution for the system of equations, the number of parameters (i.e. degrees of freedom) in the MSM needs to be increased. We tested several extensions to the simple MSM, such as additional springs or area preserving forces. The simplest and most satisfactory solution was obtained if springs with prestrain are used. In this case the remaining elements are no longer zero. In the prestrained spring model, the rest-length of the spring (i, j) does not correspond to the distance between nodes i and j in the static equilibrium of the rectangular model. The rest-length can be written as $l^0_{(i,j)} = c \left\| \mathbf{p}^0_i - \mathbf{p}^0_j \right\|$, where $\mathbf{p}^0_j$ is the position of node j in the equilibrium and c is a constant factor. The variable c adds a degree of freedom, which makes it possible to equate the stiffness matrices and solve for the spring coefficients. The matrix K_{MSM} of the model with and without prestrain is visualized in Figure 5. If the rectangle is square and
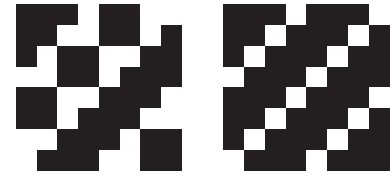

Fig. 5. On the left the stiffness matrix of the MSM without prestrain is shown. On the right the stiffness matrix of the MSM with prestrain is shown. Zeros are displayed in white and the non zeros are black.

the Poisson's ratio ν is $\frac{1}{3}$ the equations can be solved. We obtain following formulae for the spring coefficients

$$k_{edge} = \sum_e \frac{5}{16} t E$$

$$k_{diagonal} = \frac{7}{16} t E \tag{10}$$

and the following expressions hold for the rest-length

$$l^0_{edge} = \frac{6}{5} \left\| \mathbf{p}^0_i - \mathbf{p}^0_j \right\|$$

$$l^0_{diagonal} = \frac{6}{7} \left\| \mathbf{p}^0_i - \mathbf{p}^0_j \right\|. \tag{11}$$

In Equation 10, only the edge spring stiffness values must be summed, since the diagonal spring is inside the rectangle. Because of symmetries and because the diagonal spring forces should be balanced by the horizontal and vertical spring forces, only one free parameter actually is added. Stated in a more generic form, we add one degree of freedom in order to increase the flexibility of the MSM and improve the agreement in the equilibrium. It is important to note that this rectangle mass spring model is in static equilibrium, in contrast to the rectangle MSM with preload by Wang and Devarajan [22]. As mentioned above, the formulae in Equation 10 is valid for square elements.

4.2 Tetrahedron Elements

Our main concern is to model solid deformable objects for surgery simulation. From the beginning it has been our goal to arrive at expressions for 3D meshes. In the previous sections

most of the ingredients necessary to derive the important extension to 3D have been prepared. Finally, in this section formulae for tetrahedron elements are presented. In Figure 6 the tetrahedron element and a corresponding simple MSM is shown. In
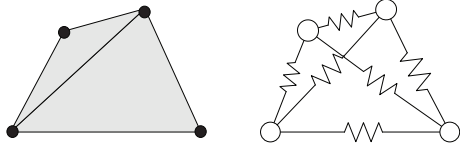

Fig. 6. On the left the FEM tetrahedron element is shown. On the right the corresponding MSM is depicted.

Appendix B the calculation of the stiffness matrix of the constant strain tetrahedron element is presented. The linearization of the MSM is analogous to the triangle and rectangle case, although now the z-coordinate also needs to be considered. The sub-matrix $A_{i,j}$ introduced in Equation 6 becomes

$$A_{i,j} = \frac{k_{(i,j)}}{l^0_{(i,j)}{}^2} \begin{pmatrix} x_i^0 - x_j^0 \\ y_i^0 - y_j^0 \\ z_i^0 - z_j^0 \end{pmatrix} \begin{pmatrix} x_i^0 - x_j^0 \\ y_i^0 - y_j^0 \\ z_i^0 - z_j^0 \end{pmatrix}^T$$

To analyze the stiffness matrices, we again transform the element into a specific position and orientation. As with the rectangle mesh, there are many zeros in the stiffness matrix of the MSM, whereas there are only few zeros in the FEM stiffness matrix. The matrices are visualized in Figure 7.

Fig. 7. The stiffness matrix of the linearized tetrahedron MSM is shown on the left. On the right the FEM stiffness matrix is shown. Zeros are displayed in white and the non zeros are black

Thus, no exact analytical solution can be found. Nevertheless, we propose two methods to find a solution. Either we can treat the problem as an optimization problem and analytically optimize a similarity metric. Alternatively, we can proceed as in the rectangle case and add degrees of freedom in order to improve the agreement between the MSM and FEM. Since the second method does not succeed in finding an exact solution, we suggest a hybrid method, which uses the additional degree of freedom and the optimization to obtain an approximate solution.

4.2.1 Optimization Approach

In order to find a MSM which approximates the reference model in an optimal way, two things will be considered. First the 3×3 submatrices of K_{CST} should be symmetric, since the corresponding submatrices of K_{MSM} are symmetric. This leads to the condition that the Poisson's ratio ν of the linear elastic reference material should be $\frac{1}{4}$. Second, the difference between the stiffness matrices should be minimal. We experimented with several similarity measures, *e.g.* the squared difference between the matrix elements or the error between the

corresponding eigenvalues. Since the results were similar, the squared difference $\epsilon(\theta)$ was chosen for simplicity. The error criterion is defined as

$$\epsilon(\theta) = \sum_{i,j} \left([K_{CST}]_{i,j} - [K_{MSM}(\theta)]_{i,j} \right)^2 .$$

Using the MATLAB Symbolic Math Toolbox we computed following formula for a regular tetrahedron

$$k_{(i,j)} = \sum_e \frac{2\sqrt{2}}{25} l E \tag{12}$$

The expression is optimal in the least squares sense, *i.e.* the squared difference error between the elements of the stiffness matrices K_{MSM} and K_{CST} is minimized.

Optimization of $\epsilon(\theta)$ for arbitrarily shaped tetrahedra can give arbitrary stiffness coefficients. This is however problematic since the spring coefficients can be negative. Especially tetrahedra with unfavorable angles as classified by Bern et al. [27], *e.g.* so-called slivers, spindles and caps, result in negative spring parameters. They have large dihedral angles and according to Shewchuk [28] are bad for linear interpolation (used in the FEM). Since negative spring coefficients are physically not plausible and cause instabilities, we slightly amend the proposed formula. Given a tetrahedral mesh we take into consideration the contribution from each adjacent tetrahedron. If a tetrahedron is not regular we calculate an equivalent edge length $\hat{l}$ from the volume. The volume V of a regular tetrahedron is $V = l^3 \frac{\sqrt{2}}{12}$. By inverting this formula, the equivalent length for each adjacent tetrahedron can be obtained as

$$\hat{l_e} = \left(V_e \frac{12}{\sqrt{2}} \right)^{\frac{1}{3}} . \tag{13}$$

Using $\hat{l_e}$ in Equation 12 we obtained good results. Generally, a better mesh quality results in a better behavior of the MSM, where quality is defined as a measure of how close to regular the tetrahedra are.

4.2.2 Hybrid Approach with Volume Preserving Forces

As already shown in Section 4.1 modifications or extensions to the MSM can improve the approximation. For the tetrahedron MSM it does not seem plausible to assume that the springs are compressed or stretched in the static equilibrium, since, unlike the rectangle case, the resulting forces would not be compensated. The simple MSM can, however, be extended by volume preserving forces. Additional forces again add more degrees of freedom to the MSM, which allows us to better approximate the FEM stiffness matrix in the operating point. Teschner et al. [29] presented an extended MSM, which includes volume preserving forces derived from a volume constraint type potential energy. The volume preserving forces are also supposed to add more realism, especially for simulating soft biological tissue. The derivation of the stiffness matrix K_V for this type of force is presented in Appendix C.2. To demonstrate the better agreement of the stiffness matrices, the patterns of the extended MSM and the FEM is shown in Figure 8. Although, still not a perfect

Fig. 8.   The stiffness matrix of the linearized tetrahedron augmented MSM with volume preserving forces is shown on the left. On the right the FEM stiffness matrix is shown. Zeros are displayed in white and the non zeros are black

match, they are now closer than in Figure 7. Using the volume preserving forces combined with an optimization approach, the derivation of the parameters is now based on minimizing

$$\epsilon(\theta) = \sum_{i,j} \left([K_{CST}]_{i,j} - [K_{MSM}(\theta)]_{i,j} - [K_V(\theta)]_{i,j} \right)^2 .$$

The resulting formulae for a regular tetrahedron are given by

$$k_{(i,j)} = \sum_e \frac{2\sqrt{2}}{21} l\, E \frac{4}{5}$$

$$k_V = \frac{\sqrt{2}}{84} l^3\, E \frac{2}{5}, \tag{14}$$

where k_V is the coefficient of the volume preserving force. Again, for arbitrary tetrahedral meshes we use the equivalent edge length $\hat{l}_e$ as defined in Equation 13.

5   EXPERIMENTS AND RESULTS

In this section we demonstrate in several experiments that the derived spring coefficients result in mass spring models, which have similar properties to a linear elastic reference model, simulated with FEM. For our experiments we use a Young's modulus of approximately 15 kPa, which corresponds to a measured value for the liver [12]. In most experiments we apply loads, resulting in quite large deformations of around ten to thirteen percent. The MSM is generally displayed in red, while the ground truth FEM deformation is shown in black. In nearly all the experiments we have the following boundary conditions. The bottom surface is fixed and a traction force is applied to the top surface, either in positive z-direction (stretch), negative z-direction (compression) or in positive y-direction (shear). Additionally, in order to provide quantitative results, we have calculated the Euclidean distance error between the nodes in the reference and the mass spring model. We give the maximum and the mean error.

5.1   Linear Elastic Membrane simulated with Equilateral Triangles

In Figure 9 stretching, compression and shear forces were applied to a MSM with an equilateral triangle mesh. The MSM behaves in a very similar way to the linear elastic reference model simulated with the FEM. The parameters of the reference model are $E = 14630 Pa$ and $\nu = 1/3$. The model consists of 39 nodes and 92 springs. The maximum (mean) error was $0.033cm$ ($0.008cm$), $0.061cm$ ($0.012cm$), and $0.098cm$

$(0.034cm)$ for the stretch, compression and shear test respectively. The object is $5.2cm$ high and is stretched approximately $11.2 - 13.6\%$.

5.2   Comparison of Methods to simulate Arbitrary Triangles

Since in typical applications it is not possible to use equilateral triangle meshes, it is necessary to validate the derived formula for arbitrary triangle shapes as well. In this experiment a rectangular object is meshed with a triangle meshing tool. Along the edges of the object the triangle quality is generally worse than inside the object. In Figure 10 we used the formula for equilateral triangles from Equation 8, whereas in Figure 11 we used the modified formula from Equation 9. The formula for equilateral triangles leads to slightly larger errors, visible at the corners of the object. The parameters of the reference model are $E = 14630 Pa$ and $\nu = 1/3$.

5.3   Linear Elastic Membrane simulated with Rectangle Mesh

In Figure 12 the MSM with spring parameters as defined in Equation 10 is compared to a linear elastic membrane simulated with constant strain rectangle elements. The parameters of the reference model are $E = 14630 Pa$ and $\nu = 1/3$. The model consists of 36 nodes and 110 springs. The maximum (mean) error was $0.076cm$ ($0.041cm$), $0.129cm$ ($0.0677cm$), $0.196cm$ ($0.066cm$) for the stretch, compression and shear test respectively. The object is $5cm \times 5cm$ in the undeformed state and was stretched and compressed approximately 12%.

5.4   Different Mesh Resolutions

To test the ability to represent an object at different resolutions using the derived spring parameters, the stretching, compression and shear experiments were carried out for the rectangle mesh model. In Figure 13 the shear force was applied to the same object, modeled at different mesh resolutions. The mesh on the left contains 20 springs, the mesh in the center has 110 springs, and the mesh on the right contains 1482 springs. The black line represents the FEM reference deformation, computed with the highest resolution. The maximum (mean) error was $0.082cm$ ($0.036cm$), $0.087cm$ ($0.033cm$) and $0.078cm$ ($0.024cm$) for a), b), and c) respectively. The results demonstrate that we can easily create models at different resolutions with the same physical properties. Previously, this would have been a difficult task. The object is $5cm \times 5cm$ in the undeformed state.

5.5   Simulation of a Two-Layer Model

To illustrate the capability to model an object consisting of several homogeneous linear elastic parts with different properties, we experimented with a two-layer model in 2D. Three example deformation simulation results are shown in Figure 14. A square plate or membrane model, which consists of two linear elastic materials is simulated. The Young's modulus of the top half of the object is $E_t = 40kPa$. The bottom half has a Young's modulus of $E_b = 4kPa$. On the left the object is stretched, in the middle it is compressed and on the right a
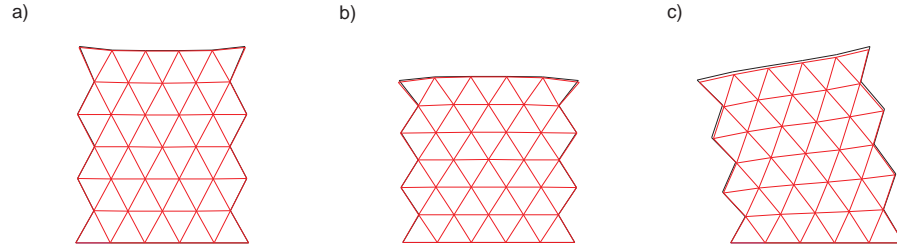
Fig. 9. Several load cases were tested on this equilateral triangular mesh: a) stretch, b) compression, c) shear. The deformation in a) corresponds to $11.2 - 13.6\%$ (measured at corner or middle node on top boundary). The spring coefficient was set using (8). The object simulated with FEM is represented by the black line. The MSM is shown in red.
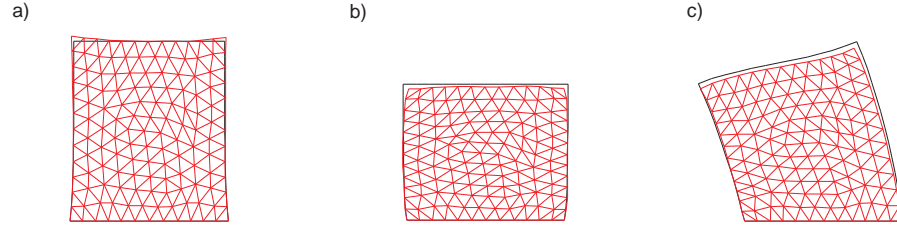

Fig. 10. Loads were applied to this triangular mesh with the original spring coefficient formula from Equation 8 derived for equilateral meshes: a) stretch, b) compression, c) shear. The deformation in a) corresponds to 13.5%. (MSM: red; FEM: black)
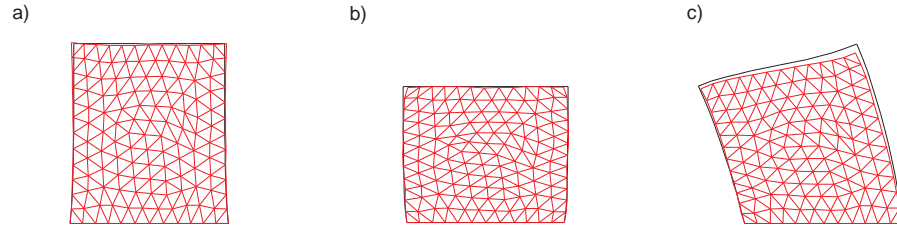

Fig. 11. Simulation results for a triangular mesh with the modified spring coefficient formula from Equation 9. The deformation in a) corresponds to 13.5%. (MSM: red; FEM: black)
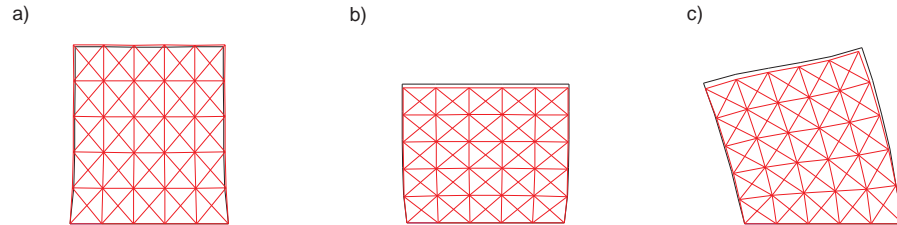

Fig. 12. Loads were applied to a rectangle mesh with spring coefficients set using Equation 10. The object is stretched (12%) in Figure a) and compressed (12%) in b). Shearing is shown in Figure c). (MSM: red; FEM: black)

shearing force is applied. The simulation results qualitatively show that the corresponding MSM can simulate the behavior of the reference model quite accurately. The MSM consists of 49 nodes and 156 springs.

5.6 Linear Elastic Solid simulated with a Simple MSM

In this experiment we simulate a linear elastic solid with constant strain tetrahedra using the FEM and compare the simulation with a corresponding MSM. The spring coefficients are set using Equation 12 with the equivalent edge length $\hat{l}$ from Equation 13. In Figure 15 a cylindrical object and in Figure 16 a high resolution cylinder with an empty spherical hole is simulated. The maximum (mean) error in Figure 15 was $0.039cm$ $(0.013cm)$, $0.111cm$ $(0.025cm)$ and $0.088cm$ $(0.029cm)$ for the stretch, compression and shear test respectively. The maximum (mean) error in Figure 16 was $0.039cm$ $(0.012cm)$, $0.065cm$ $(0.013cm)$ and $0.100cm$ $(0.035cm)$ for the stretch, compression and shear test respectively. The cylinders in both Figures have a radius of $1cm$ and a height of $2cm$ in the undeformed state. The stretching deformation in Figure 16 a) corresponds to 15%.

5.7 Large Deformation

Since the linear elastic model can be inaccurate for large displacements $(> 10\%)$ it is obviously not the ideal reference
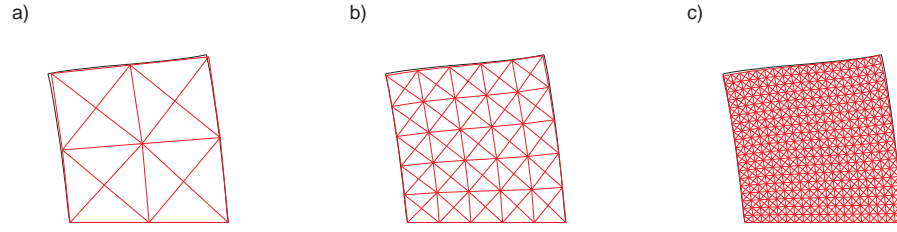
a) b) c)

Fig. 13. Simulation results for the rectangle mesh. The shear experiment simulated using different mesh resolutions. In a) a mesh with 4 rectangle elements is used, in b) a mesh with 25 rectangles and in c) a mesh with 361 rectangles are shown.
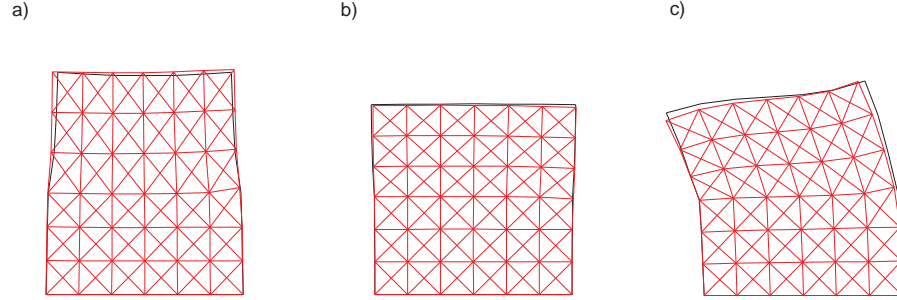
a) b) c)

Fig. 14. A two-layer model - the top layer (top three rows of rectangles) is much softer than the bottom layer (factor 10). (MSM: red; FEM: black). Different load cases were applied: in a) stretch, b) compression, c) shear.
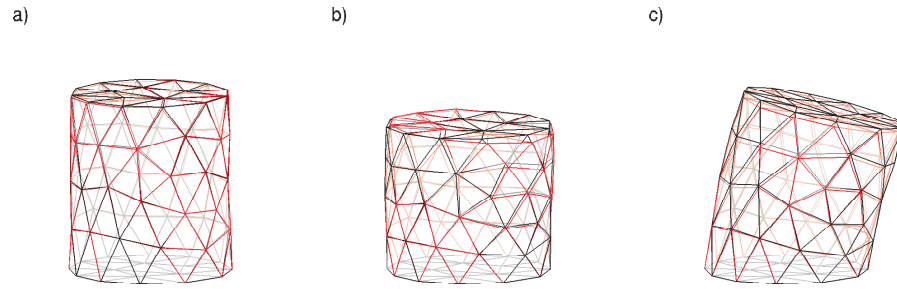
a) b) c)

Fig. 15. A cylindrical object consisting of 91 nodes, 435 springs and 274 tetrahedra. The spring coefficients are set according to Equation 12. (MSM: red; FEM: black). Three load cases were applied: in a) stretch, b) compression, c) shear.
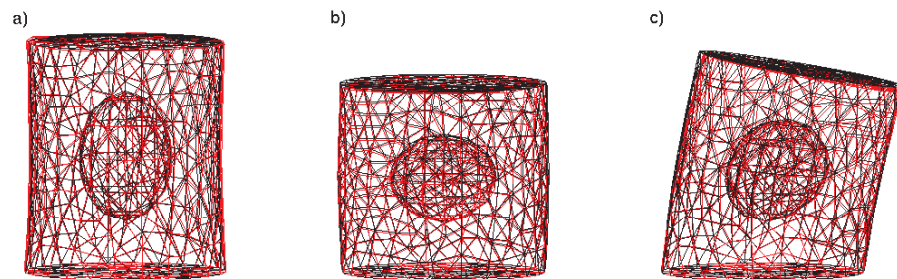
a) b) c)

Fig. 16. A cylindrical object with an empty space inside is deformed. The object is represented by a mesh consisting of 873 nodes and 3807 tetrahedra. The spring coefficients are set according to Equation 12. (MSM: red; FEM: black). Different load cases were applied: in a) stretch, b) compression, c) shear.

model for these conditions. The rotational artifacts which occur in linear elasticity should optimally not be introduced by our method. In order to verify that the MSM does not reproduce these errors, we conducted several experiments. In Figure 17 we compared a MSM to a linear elastic model and a geometrically non-linear model with the same Young's modulus and Poisson ratio. For large deformations and rotations the MSM behaves more like the non-linear model. This is due to the non-linearity of the MSM.

a)   b)
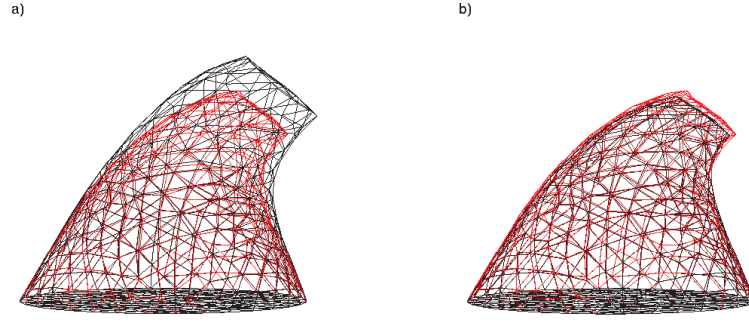

Fig. 17. A cone shaped object, fixed at the bottom, with large shearing forces applied at the top surface. The spring coefficients are set according to Equation 12. (MSM: red; Reference: black). In $a)$ the reference material is simulated using a linear elastic law, while in $b)$ it is simulated with a geometrically non-linear model (Green-Lagrange strain measure). The mesh consists of 982 nodes, 5840 springs and 4407 tetrahedra.

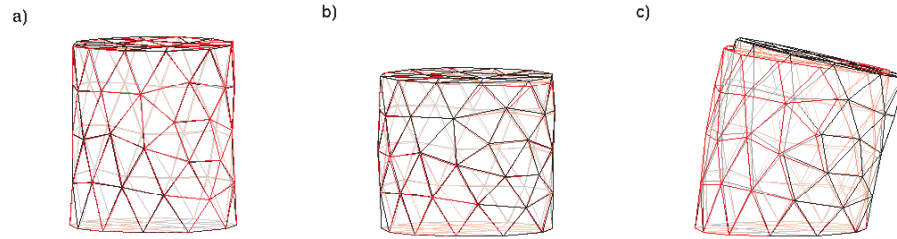a)   b)   c)

Fig. 18. A cylinder-shaped object consisting of 91 nodes, 435 springs and 274 tetrahedra. The spring coefficients are set according to Equation 14. (MSM: red; FEM: black). Different load cases were applied: in a) stretch, b) compression, c) shear.

5.8 Linear Elastic Solid simulated with a MSM with Volume Preserving Forces

In Figure 18 the short cylinder was simulated with a MSM with volume preserving forces according to Equation 14. The maximum (mean) error was $0.029cm$ ($0.009cm$), $0.073cm$ ($0.018cm$) and $0.183cm$ ($0.080cm$) for the stretch, compression and shear test respectively. The cylinder has a radius of $1cm$ and a height of $2cm$ in the undeformed state. For the stretch and compression test, the maximum and mean errors are slightly smaller than without volume preserving forces. For the shear test however, the errors are noticeably larger. One possible explanation is that the chosen volume preserving force is not optimal. It might not be appropriate, since the reaction force depends heavily on the deformation direction. For instance if a corner node of a tetrahedron is moved parallel to the opposite face, no reaction force results from the volume preservation. Alternative volume preserving forces might be better in this respect (*e.g.* [6]). Moreover, the observed stiffening in the shear test resembles the effects of geometric non-linearity, which is not included in the finite element analysis, because it is based on the small strain assumption.

5.9 Soft Tissue Simulation for Surgery Simulation

As an example application in Figure 19 a) a scene from our hysteroscopy simulator is shown [30, 31]. On the left the endoscopic view of a uterine myoma model is shown. The underlying mesh representation is depicted on the right. We simulated the deformation of the myoma using the linear FEM (in black) and a MSM (in red) in Figure 19 b), leading to very similar results. The mesh consists of 391 elements.

6 CONCLUSIONS AND FUTURE WORK

In this contribution we presented a new method to derive analytical expressions for spring coefficients in MSM. The formulae were calculated by linearizing the mass spring model forces in the node displacements. This results in equations, which are equivalent to the ones typically obtained using the FEM for linear elasticity. In matrix notation it can be identified that the stiffness matrix of the reference model must be equal to the stiffness matrix of the linearized MSM in the equilibrium position.

We presented expressions, which are valid for triangle, rectangle and tetrahedron meshes. In the case of the rectangle mesh, we used a spring model with prestrain. This extension added one extra degree of freedom which improves the approximation between the stiffness matrices of the MSM and the FEM-based model. For the tetrahedron element we defined a similarity measure between the FEM and linearized MSM stiffness matrices. This similarity measure was optimized analytically to obtain formulae for the spring coefficients. To improve the operating point approximation between the stiffness matrices, an extended MSM with volume preserving forces was used. This again added one degree of freedom for the optimization.

To validate the derived expressions we simulated various objects with a MSM and separately with the FEM as ground truth. The objects were discretized with triangular, rectangular or tetrahedral meshes. For all objects we performed a stretch, compression and shear test. Stretching and compression strains of approximately ten to thirteen percent were applied. Generally, the MSM deformations were very close to the FEM reference. Although the stiffness matrix of the tetrahedron could only be approximated, the experimental results suggest that the
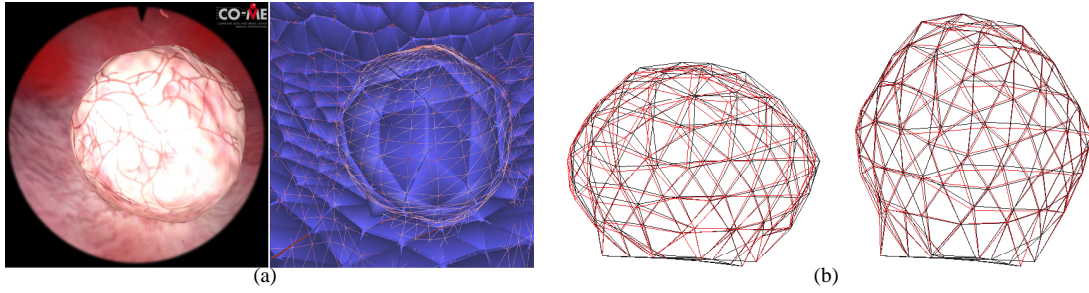
Fig. 19. In a) a snapshot of a myoma (pathology) inside the uterus from our hysteroscopy simulator is shown. The surgeon would push and pull the myoma in order to test the consistency. In b) the myoma was first statically pushed, then pulled from the top. First it was simulated with linear FEM (black) and then with a MSM (red).

behavior of the reference model and the MSM is very similar. The extended tetrahedron MSM with volume preserving forces slightly improved the behavior for stretching and compression compared to the simple MSM, but was less accurate for shearing. This can possibly be explained by an inappropriate choice for the volume preservation term. Expressions for alternative volume or shape preserving forces could easily be derived using the described approach. Additional tests demonstrated that it is possible to simulate models consisting of multiple different materials and at different resolutions. Finally, the mesh size is not a limiting factor as in the case of the data-driven parameter identification methods.

On a broader scope our motivation is to find spring parameters, which allow us to simulate soft tissue in real-time in our hysteroscopy training simulator [30, 31] and our haptic interaction test-bed [32]. For this specific purpose it is necessary to measure the elastic or visco-elastic properties of real tissue in deformation experiments. The reference material in this case is non-linear and the small strain assumption usually not valid. Since the derivation of the parameters was based on an operating point approximation, *i.e.* the tangents of the forces in the equilibrium position are equal for the reference and mass spring model, the MSM will only behave like the reference model for small strains. In general it will not behave like the geometrically linear reference model for large deformation. This might however not even be desirable, since the geometrically linear FEM is very inaccurate for large deformations and rotations. Experimentally, we have found that for large rotations and deformations the MSM behaves more like a geometrically non-linear model (Green-Lagrange strain), with material linearity.

The results are limited by the fact that the formulae are only valid for specific Poisson ratios. This seems to be rather a limitation of the MSM itself, since in a simple triangular or tetrahedral mesh, there is no mechanism to control the Poisson ratio. Additionally, the formulae are optimal only for well shaped elements, although we suggested how they could be modified for arbitrary element shapes.

For future work we plan to use and extend our method to find expressions for different reference materials, for instance for Neo-Hookean or Mooney-Rivlin material. It would also be interesting to use higher order elements as a reference model, for instance quadratic (6-node) triangles or quadratic tetrahedra. Use of quadratic elements implies a higher connectivity

between the nodes of the MSM. Another interesting question is related to the expressions derived for the tetrahedron. The chosen volume preserving force is probably not optimal. We are planning to compare this volume preserving force with others [6]. Last but not least, it would be interesting to use the same approach to derive formulae for the spring damping coefficients.

APPENDICES

A PLANE STRESS LINEAR ELASTICITY

Hooke's Law states that there is a linear relationship between the stresses σ and strains ϵ. In 1D this corresponds to the spring model. For solids the relation can be written in matrix form as $\sigma = D\epsilon$.

For the 2D case there are two simplifications which result in different models. The so-called plane stress case assumes stresses in the z-direction are negligible, $\sigma_{xz} = \sigma_{yz} = \sigma_{zz} = 0$, whereas the plane strain case assumes the strains in z-direction are negligible. The constitutive equations for the plane stress case are

$$
\begin{pmatrix} \sigma_{xx} \\ \sigma_{yy} \\ \sigma_{xy} \end{pmatrix} = \frac{E}{1-\nu^2} \begin{bmatrix} 1 & \nu & 0 \\ \nu & 1 & 0 \\ 0 & 0 & 1-\nu \end{bmatrix} \begin{pmatrix} \epsilon_{xx} \\ \epsilon_{yy} \\ \epsilon_{xy} \end{pmatrix},
$$

where E is the Young's modulus and ν is the Poisson's ratio. The plane stress case is used to model a thin material such as a plate or membrane subject to in-plane loading. A slightly different form results for plane strain. The plane strain case deals with the case of very thick objects where in-plane strains are much greater than normal strains.

B FEM STIFFNESS MATRIX FOR TETRAHEDRON ELEMENT

Zienkiewicz and Taylor [24] describe how the stiffness matrix of the constant strain tetrahedron (4-node tetrahedron with linear interpolation functions) can be calculated for a linear elastic material. The tetrahedron element shape functions N_i are the tetrahedral coordinates. They are interpolation functions defined inside and on the boundary of the tetrahedron. Using the iso-parametric formulation they can be defined by the following

relation

$$\begin{pmatrix} 1 \\ x \\ y \\ z \end{pmatrix} = \begin{bmatrix} 1 & 1 & 1 & 1 \\ x_1 & x_2 & x_3 & x_4 \\ y_1 & y_2 & y_3 & y_4 \\ z_1 & z_2 & z_3 & z_4 \end{bmatrix} \begin{pmatrix} N_1 \\ N_2 \\ N_3 \\ N_4 \end{pmatrix}.$$

The displacements are interpolated using these shape functions

$$u(x,y,z) = \sum_{i=1}^{4} u_i \, N_i(x,y,z) \qquad (15)$$

where u_i are the unknown displacements in x direction at the vertices. The displacements in y and z-direction can be computed in the same manner. Using following definition for (small) strains

$$\epsilon = \begin{pmatrix} \frac{\partial u}{\partial x} & \frac{\partial v}{\partial y} & \frac{\partial w}{\partial z} & \frac{\partial u}{\partial y} + \frac{\partial v}{\partial x} & \frac{\partial v}{\partial z} + \frac{\partial w}{\partial y} & \frac{\partial w}{\partial x} + \frac{\partial u}{\partial z} \end{pmatrix}^T$$

and Equation 15 we can easily derive the linear relationship

$$\epsilon = B\,\mathbf{d} \qquad (16)$$

where $\mathbf{d}$ is a vector that contains the unknown displacements $u_1, v_1, w_1, u_2, \cdots, u_4, v_4, w_4$. With the linear stress-strain relationship $\sigma = D\,\epsilon$, the potential energy of the solid $E_{pot} = \int_V \frac{1}{2}\sigma^T \epsilon \, dV$ becomes

$$E_{pot} = \int_V \frac{1}{2}\epsilon^T D\epsilon \, dV,$$

where the term inside the integral is the energy density. Using Equation 16 the force equation can be written as

$$\mathbf{f} = \int_V B^T D B \, dV \, \mathbf{d},$$

The integral on the right side is identified as the stiffness matrix K. Since the matrix B is constant for the 4-node tetrahedron, the stiffness matrix becomes

$$K = \int_V B^T D B \, dV = B^T D B\, V\,.$$

C Stiffness Matrix derived from Constraint Type Potential Energy

Particle systems are often modeled using forces which depend on a subset of the particles. One class of forces of this type can be derived from a potential energy function. First, we define the forces and stiffness matrix for a general constraint type potential energy like in Baraff and Witkin [3]. We then derive the stiffness matrix for a tetrahedron volume preserving force.

C.1 Constraint Type Potential Energy

Given a condition $C(\mathbf{x})$ which should be zero, we write an energy function $E_C = k\frac{1}{2}C^2(\mathbf{x})$ where k is a stiffness constant and $\mathbf{x} = (\mathbf{p}_1, \mathbf{p}_2, \cdots, \mathbf{p}_N)$ is a vector of all the particle positions. The particle forces arising from this energy are defined as the

gradient of the potential energy, *i.e.* the reaction force at particle i is

$$\mathbf{f}_i = \frac{\partial E_C}{\partial \mathbf{p}_i} = k\, C(\mathbf{x}) \frac{\partial C(\mathbf{x})}{\partial \mathbf{p}_i}. \qquad (17)$$

The force-vector $\mathbf{f}$ is sparse if the condition only depends on some of the particle positions. The matrix $K = \frac{\partial \mathbf{f}}{\partial \mathbf{x}}$ is also sparse if C does not depend on all the particle positions. The matrix K is the Jacobian of the force vector and the Hessian of the potential energy with respect to the particle positions. It is usually called the stiffness matrix. K can be written in block form, where each block $K_{i,j} = \partial^2 E_C / \partial \mathbf{p}_i \partial \mathbf{p}_j$ is a 2×2 matrix in 2D or a 3×3 matrix in 3D. The nonzero entries of K are $K_{i,j}$ for all pairs of particles i and j that C depends on. The stiffness matrix $K_{i,j}$ is

$$K_{i,j} = k\left(\frac{\partial C(\mathbf{x})}{\partial \mathbf{p}_i} \frac{\partial C(\mathbf{x})}{\partial \mathbf{p}_j}^T + \frac{\partial^2 C(\mathbf{x})}{\partial \mathbf{p}_i \partial \mathbf{p}_j} C(\mathbf{x}) \right). \qquad (18)$$

In the static equilibrium position the condition C usually is zero. Therefore, in the equilibrium the second term in the expression above is zero. The stiffness matrix in this case is simply the outer product of the gradient of the potential energy with respect to the particle positions.

C.2 Volume Preserving Potential Energy

The stiffness matrix of the volume preserving force for a tetrahedron defined by the potential energy [29] $E_V = k_V \frac{1}{2V_0^2}(V(\mathbf{x}) - V_0)^2$ where $\mathbf{x} = (\mathbf{p}_1, \mathbf{p}_2, \mathbf{p}_3, \mathbf{p}_4)$ are the vertices of the tetrahedron, V is the volume and V_0 is the volume in the static equilibrium. First we calculate the gradient of the condition $C = (V(\mathbf{x}) - V_0)/V_0$ with respect to the corner vertices. Based on this result we can derive the forces and the stiffness matrix. The volume of the tetrahedron is $1/6(\mathbf{p}_2 - \mathbf{p}_1)((\mathbf{p}_3 - \mathbf{p}_1) \times (\mathbf{p}_4 - \mathbf{p}_1))$. For instance taking the gradient of C with respect to $\mathbf{p}_2$ we get

$$\frac{\partial C}{\partial \mathbf{p}_2} = \frac{\partial V(\mathbf{x})}{\partial \mathbf{p}_2} \frac{1}{V_0} = \frac{1}{6V_0}(\mathbf{p}_3 - \mathbf{p}_1) \times (\mathbf{p}_4 - \mathbf{p}_1),$$

which is a vector with direction perpendicular to the triangle opposite vertex 2, with a magnitude of two times the area of the triangle. Similarly, the gradients with respect to the other vertices can be calculated. The 12×1 gradient vector with respect to $\mathbf{x}$ is

$$\frac{\partial C}{\partial \mathbf{x}} = \frac{1}{6V_0} \begin{pmatrix} (\mathbf{p}_2 - \mathbf{p}_4) \times (\mathbf{p}_3 - \mathbf{p}_4) \\ (\mathbf{p}_3 - \mathbf{p}_1) \times (\mathbf{p}_4 - \mathbf{p}_1) \\ (\mathbf{p}_4 - \mathbf{p}_2) \times (\mathbf{p}_1 - \mathbf{p}_2) \\ (\mathbf{p}_1 - \mathbf{p}_3) \times (\mathbf{p}_2 - \mathbf{p}_3) \end{pmatrix}.$$

The 12×12 stiffness matrix in the equilibrium position is then easily calculated using 18.

REFERENCES

[1] D. Terzopoulos, J. Platt, A. Barr, and K. Fleischer, "Elastically deformable models," *SIGGRAPH Comput. Graph.*, vol. 21, no. 4, pp. 205–214, 1987.

[2] D. Terzopoulos and K. Fleischer, "Modeling inelastic deformation: viscolelasticity, plasticity, fracture," in *SIGGRAPH '88: Proceedings of the 15th annual conference on Computer graphics and interactive techniques*. New York, NY, USA: ACM Press, 1988, pp. 269–278.

[3] D. Baraff and A. Witkin, "Large steps in cloth simulation," in *SIGGRAPH '98: Proceedings of the 25th annual conference on Computer graphics and interactive techniques*. New York, NY, USA: ACM Press, 1998, pp. 43–54.

[4] X. Provot, "Deformation constraints in a spring-mass model to describe rigid cloth behavior," in *Proceedings of Graphics Interface*, 1995, pp. 147–154.

[5] K. Kähler, J. Haber, and H.-P. Seidel, "Geometry-based muscle modeling for facial animation," in *Proceedings of Graphics Interface*. Toronto, Ont., Canada, Canada: Canadian Information Processing Society, 2001, pp. 37–46.

[6] W. Mollemans, F. Schutyser, J. V. Cleynenbreugel, and P. Suetens, "Fast soft tissue deformation with tetrahedral mass spring model for maxillofacial surgery planning systems," in *In Proceedings of Medical Image Computing and Computer-Assisted Intervention, MICCAI 2004, Springer LNCS*, 2004, pp. 371–379.

[7] S. Zhang, L. Gu1, P. Huang, and J. Xu, "Real-time simulation of deformable soft tissue based on mass-spring and medial representation," in *Computer Vision for Biomedical Image Applications: First International Workshop, CVBIA 2005*. Springer-Verlag, 2005, pp. 419–426.

[8] J. Brown, S. Sorkin, J.-C. Latombe, K. Montgomery, and M. Stephanides, "Algorithmic tools for real-time microsurgery simulation," *Medical Image Analysis*, vol. 6, no. 3, pp. 289–300, 2002.

[9] H. Delingette and N. Ayache, "Soft tissue modeling for surgery simulation," in *Computational Models for the Human Body*, ser. Handbook of Numerical Analysis (Ed : Ph. Ciarlet), N. Ayache, Ed. Elsevier, 2004, pp. 453–550.

[10] B. Lee, D. C. Popescu, B. Joshi, and S. Ourselin, "Efficient topology modification and deformation for finite element models using condensation," *Stud Health Technol Inform*, vol. 119, pp. 299–304, 2006.

[11] Y. Zheng and A. Mak, "Effective elastic properties for lower limb soft tissues from manual indentation experiment," *Rehabilitation Engineering, IEEE Transactions on*, vol. 7, no. 3, pp. .257–267, 1999.

[12] M. P. Ottensmeyer, "In vivo measurement of solid organ visco-elastic properties." *Stud Health Technol Inform*, vol. 85, pp. 328–333, 2002.

[13] O. Deussen, L. Kobbelt, and P. Tucke, "Using simulated annealing to obtain good nodal approximations of deformable objects," in *Computer Animation and Simulation*, 1995, pp. 30–43.

[14] J. Louchet, X. Provot, and D. Crochemore, "Evolutionary identification of cloth animation models," in *Computer Animation and Simulation*, 1995, pp. 44–54.

[15] K. S. Bhat, C. D. Twigg, J. K. Hodgins, P. K. Khosla, Z. Popovic, and S. M. Seitz, "Estimating cloth simulation parameters from video," in *SCA '03: Proceedings of the 2003 ACM SIGGRAPH/Eurographics symposium on Computer animation*. Aire-la-Ville, Switzerland, Switzerland: Eurographics Association, 2003, pp. 37–51.

[16] G. Bianchi, M. Harders, and G. Székely, "Mesh topology identification for mass-spring models," in *Medical Image Computing and Computer-Assisted Intervention MICCAI 2003*, vol. 1, November 2003, pp. 50–58.

[17] G. Bianchi, B. Solenthaler, G. Székely, and M. Harders, "Simultaneous topology and stiffness identification for mass-spring models based on fem reference deformations," in *Medical Image Computing and Computer-Assisted Intervention MICCAI 2004*, C. Barillot, Ed., vol. 2. Springer, November 2004, pp. 293–301.

[18] R. Nogami, H. Noborio, F. Ujibe, and H. Fujii, "Precise deformation of rheologic object under msd models with many voxels and calibrating parameters," in *Robotics and Automation, 2004. Proceedings. ICRA '04. 2004 IEEE International Conference on*, vol. 2, 2004, pp. 1919–1926 Vol.2.

[19] A. V. Gelder, "Approximate simulation of elastic membranes by triangulated spring meshes," *J. Graph. Tools*, vol. 3, no. 2, pp. 21–42, 1998.

[20] A. Maciel, R. Boulic, and D. Thalmann, "Deformable tissue parameterized by properties of real biological tissue," in *Surgery Simulation and Soft Tissue Modeling: International Symposium, IS4TM '03, LNCS*. Springer, 2003.

[21] O. Etzmuss, J. Gross, and W. Strasser, "Deriving a particle system from continuum mechanics for the animation of deformable objects," *Visualization and Computer Graphics, IEEE Transactions on*, vol. 9, pp. 538–550, 2003.

[22] X. Wang and V. Devarajan, "1d and 2d structured mass-spring models with preload," *The Visual Computer*, vol. 21, no. 7, pp. 429–448, 2005.

[23] X. Wang, Y. Shen, and V. Devarajan, "Physically accurate mesh simulation in a laparoscopic hernia surgery simulator," in *Medicine Meets Virtual Reality 14*. IOS Press, 2006, 2006, pp. 568–573.

[24] O. Zienkiewicz and R. Taylor, *The Finite Element Method, Volume 1 - The Basics*. Elsevier, 2000.

[25] D. L. Logan, *A First Course in the Finite Element Method*. Brooks/Cole, 2002.

[26] "MATLAB Symbolic Math Toolbox 3.1.4," http : / / www . mathworks . com / products / symbolic/.

[27] M. Bern, P. Chew, D. Eppstein, and J. Ruppert, "Dihedral bounds for mesh generation in high dimensions," in *SODA '95: Proceedings of the sixth annual ACM-SIAM symposium on Discrete algorithms*. Philadelphia, PA, USA: Society for Industrial and Applied Mathematics, 1995, pp. 189–196.

[28] J. R. Shewchuk, "What is a good linear element? interpolation, conditioning, and quality measures," in *Proceedings, 11th International Meshing Roundtable*, September 2002, pp. 115–126.

[29] M. Teschner, B. Heidelberger, M. Muller, and M. Gross, "A versatile and robust model for geometrically complex deformable solids," in *Proc. of the Computer Graphics International*, 2004, pp. 312–319.

[30] M. Harders, M. Bajka, U. Spaelter, S. Tuchschmid, H. Bleuler, and G. Szkely, "Highly-realistic, immersive training environment for hysteroscopy," in *Medicine Meets Virtual Reality*, J. W. et al., Ed., vol. 14. IOS Press, January 2006, pp. 176–181.

[31] S. Tuchschmid, M. Grassi, D. Bachofen, P. Früh, M. Thaler, G. Szkely, and M. Harders, "A flexible framework for highly-modular surgical simulation systems," in *Biomedical Simulation: Third International Symposium, ISBMS 2006, Zurich, Switzerland, July 10-11, 2006*, ser. Lecture Notes in Computer Science, vol. 4072. Springer Berlin / Heidelberg, July 2006, pp. 84 – 92.

[32] P. Leškovský, M. Harders, and G. Székely, "Assessing the fidelity of haptically rendered deformable objects," in *Haptic Interfaces for Virtual Environment and Teleoperator Systems, 2006 14th Symposium on*, 2006, pp. 19–25.

Bryn Lloyd studied electrical engineering and information technology at the Swiss Federal Institute of Technology (ETH) in Zürich, where he received a the MSc in electrical engineering and information technology in 2005. Currently he is working on his PhD at the Computer Vision Laboratory at the ETH in Zürich. His recent work includes topics in modeling deformable objects for soft tissue models used in surgery simulation.

Gábor Székely graduated from the Technical University of Budapest in chemical engineering in 1974 and from the University of Budapest in Applied Mathematics in 1981. He obtained his Ph.D. in analytical chemistry in 1985 from the Technical University of Budapest. Currently he is associate professor for medical image analysis and visualization at the Computer Vision Laboratory of the ETH Zürich and developing image analysis, visualization and simulation methods for computer support of medical diagnosis, therapy, training and education.

Matthias Harders studied Computer Science with focus on Medical Informatics at the University of Hildesheim (Germany), Technical University of Braunschweig (Germany) and University of Houston (USA). He finished his doctoral thesis on visual-haptic medical segmentation at ETH Zürich (Switzerland) in 2002. Currently, he is lecturer and senior researcher at the Computer Vision Lab of ETH Zürich, as well as leader of the Virtual Reality in Medicine Group. His research focuses on surgical simulation, human computer interaction with medical data, and haptic interfaces. He is a member of the IEEE.